Comparison of asphalt mixtures containing polymeric compounds and polymer-modified bitumen based on the VECD theory

(Article begins on next page)

15 October 2024

1   **Comparison of asphalt mixtures containing polymeric compounds and polymer-**
2   **modified bitumen based on the VECD theory**

3

4   Sara Spadoni,[1,*] Lorenzo Paolo Ingrassia,[1] Douglas Mocelin,[2] Y. Richard Kim,[2] Francesco
5   Canestrari[1]

6   [1] Department of Civil and Building Engineering, and Architecture (DICEA), Università Politecnica
7   delle Marche, Ancona, Italy.

8   [2] Department of Civil, Construction, and Environmental Engineering, North Carolina State
9   University, Raleigh, NC, USA.

10 * Corresponding author: Sara Spadoni, s.spadoni@pm.univpm.it https://orcid.org/0000-0003-0563-
11 6473

12

13 **Abstract**

14 The 'dry' method that can be used to produce modified asphalt mixtures is a less expensive, less
15 energy-consuming, and faster process than the well-established 'wet' method. Moreover, the dry
16 method allows the incorporation of hard plastics, even those plastics obtained from waste products.
17 Although researchers agree that the dry method can improve the stiffness and rutting resistance (i.e.,
18 high-temperature performance) of asphalt mixtures, they have conflicting opinions regarding
19 mixture fatigue and cracking resistance. In this regard, this paper aims to evaluate, through the
20 application of viscoelastic continuum damage theory, the fatigue behavior of two compound asphalt
21 mixtures that have been modified using the dry method. One of the studied compounds is composed
22 of plastomeric polymer and the other is composed of waste plastic with the addition of graphene. A
23 reference mixture containing polymer-modified bitumen (representing the wet modification
24 method) was used for comparison. The experimental program involved dynamic modulus tests and
25 uniaxial cyclic fatigue tests of laboratory-compacted specimens and cores extracted from full-scale
26 field test sections. The test results from the laboratory-compacted specimens and field cores were
27 input to FlexPAVE[TM] for pavement performance simulations. Under the same volumetric
28 conditions, the three dense-graded mixtures broadly had comparable stiffness and fatigue resistance
29 values at the material level. However, in the pavement-level simulations, the reference mixture
30 exhibited much less damage after 30 years of service than the compound mixtures. Concerning the
31 field test track, the air void contents of the mixtures varied due to workability issues related to the
32 presence of the compounds. Optimum performance was obtained for asphalt layers that could be
33 characterized by an intermediate stiffness level that ensured an adequate load distribution without
34 negative consequences for the mixture's fatigue resistance and thermal resistance.

35

36 **Keywords:** Polymer modification, waste plastic, viscoelastic continuum damage (VECD), field test
37 track, FlexPAVE[TM]

1. Introduction

Within the framework of pavement engineering, researchers are currently studying new processes and materials that could improve environmental sustainability and lower production costs and thus improve affordability for industries and asphalt plants. Polymer materials, such as styrene-butadiene-styrene (SBS) and ethylene vinyl acetate (EVA), are widely used as bitumen modifiers because they enhance the mixture's rutting and fatigue resistance and mitigate its susceptibility to temperature variations [1][2][3][4]. Such polymers usually are *ad hoc* engineered and added to the asphalt binder using the 'wet' modification method, which consists of blending the polymer with the binder first at a high temperature and then mixing the modified bitumen with the aggregate [5]. Because the wet method aims to ensure complete dispersion and chemical modification, the polymers used for this purpose should have a melting point that is lower than the production temperature, and special equipment is needed during transport and storage to avoid phase separation [5][6][7].

An alternative way to modify asphalt mixtures is the 'dry' method. In this case, the polymer is added and mixed with hot aggregate directly in the asphalt plant prior to the addition of the binder [5][6]. Therefore, this modification method is suitable also for polymers, such as hard plastics, that have a melting point that is comparable to the production temperature. This dry method reduces costs and energy consumption because there is no risk of binder phase separation [6][8][9]. However, the dry method implies less control of the binder/mixture properties.

In addition, the dry method enhances pavement sustainability because the modification process can employ polymeric compounds obtained from waste plastics. In this way, the huge amount of plastic currently sent to incineration facilities or landfills can be reduced, thereby mitigating serious negative impacts on the quality of air, water, and the environment [6][10]. Waste plastics are complex materials that typically are composed of many different grades of plastic, which can complicate their homogenization within the asphalt mixture and compatibility with bitumen [6][11]. The most common plastics found in municipal solid waste are polyethylene and polypropylene [5][11], both of which are known to increase the stiffness and rutting resistance of asphalt mixtures and reduce their susceptibility to thermal loading [12][13][14][15][16]. However, to date, researchers have not reached consensus regarding the impact of polymeric compounds on the fatigue and cracking resistance of asphalt mixtures [5], mainly because the resistance to fatigue and cracking could be diminished by the increase in stiffness caused by the addition of polymer/plastic [8]. As fatigue cracking is one of the major distress types for asphalt pavements over the course of their service life, it needs to be investigated carefully in the context of asphalt mixture modification.

An advanced and reliable method to predict the fatigue performance of asphalt mixtures is based on viscoelastic continuum damage (VECD) theory. VECD theory is built on three fundamental concepts: continuum damage mechanics, the elastic–viscoelastic correspondence principle, and the time-temperature superposition principle with growing damage. Continuum damage mechanics is based on the work potential theory [17] for modeling the effects of microcracks via internal state variables, which allows the material to be considered as a continuous and homogeneous body [18]. The elastic–viscoelastic correspondence principle is based on the pseudo-strain concept, which allows to reduce the viscoelastic behavior of the material into the corresponding elastic behavior [17][19]. The time-temperature superposition principle with growing damage (and viscoplastic

80 strain) takes into account the combined effects of time/rate and temperature, even outside the
81 viscoelastic domain of the material's behavior [20]. The Simplified VECD (S-VECD) model is an
82 approach that allows the fatigue performance of a mixture to be characterized based on the results
83 of uniaxial cyclic fatigue tests and dynamic modulus tests [21]. The mechanistic-based predictive
84 capability of the S-VECD model distinguishes it from conventional fatigue modeling approaches
85 where individual index parameters are empirically defined [22]. Moreover, the S-VECD model
86 properties obtained from laboratory tests can be used directly as input data for pavement
87 performance simulations carried out using FlexPAVE^{TM} software, which allows the prediction of
88 the long-term fatigue performance of the pavement [23][24].

89 Given this background, the aim of this study is to evaluate the fatigue performance of three mixtures
90 based on the S-VECD modeling approach. A reference mixture (coded as H) that contains SBS
91 polymer-modified bitumen represents the wet modification method and two mixtures that contain
92 compounds (coded as GC and PC, respectively) represent the dry modification method. The GC
93 compound was made of recycled plastic with graphene and the PC compound was made of
94 plastomeric polymers. An open-graded mixture with SBS polymer-modified bitumen (coded as OG),
95 typically used for wearing layers, also was studied. First, the laboratory-compacted mixture
96 specimens were tested. Then, specimens from a full-scale field test track were investigated to evaluate
97 the effects of compaction in the field. Finally, pavement simulations were carried out using
98 FlexPAVE^{TM} under three scenarios in which the material properties of the asphalt layers, which were
99 set as inputs, were varied. In this regard, the OG mixture was studied mainly to reproduce the
100 pavement structure of the field test track in the FlexPAVE^{TM} simulations. Note that the S-VECD
101 modeling approach has never been used before to study the fatigue behavior of asphalt mixtures
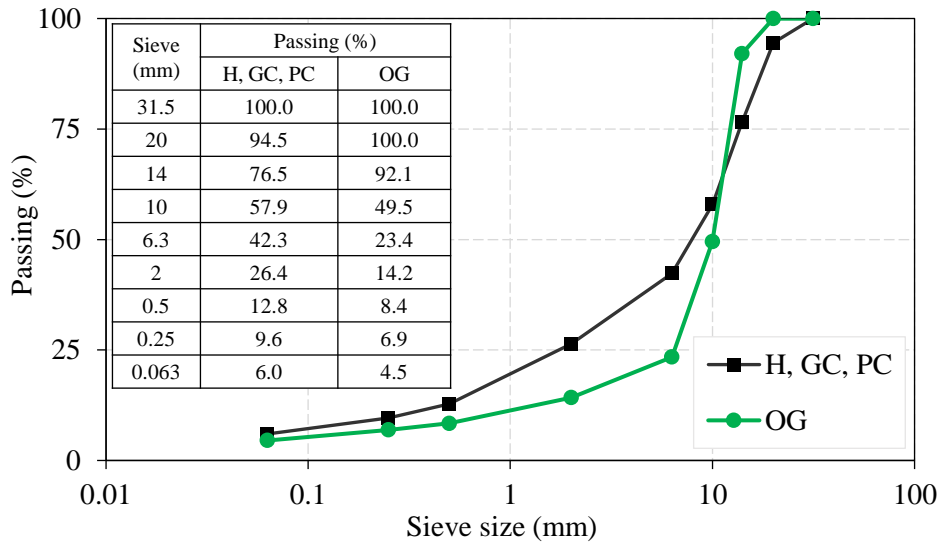102 modified with plastics via the dry method.

103 This study is part of a larger project in which, first, D'Angelo et al. assessed the rheological
104 behavior and adhesion properties of the same modified binders in this study [25]. Then, Cardone et
105 al. investigated the effects of modification using the same two compound mixtures (GC and PC) at
106 the mixture level [26]. Specifically, Cardone et al. evaluated the stiffness, rutting resistance, and
107 fatigue resistance of the same mixtures tested in this study using a traditional performance-related
108 approach based on conventional tests (i.e., indirect tensile tests and triaxial cyclic tests) and
109 performed Falling Weight Deflectometer (FWD) tests at the field test track [26]. The findings of
110 these previous studies are recalled in the following sections to enrich the discussion of the results
111 obtained in this investigation.

112 **2. Experimental program**
113 *2.1. Materials*
114 The dense-graded asphalt mixtures investigated in this study, H, GC, and PC, are the same as the
115 mixtures investigated by Cardone et al. [26]. The aggregate gradation, reported in **Figure 1**, is the
116 same for the three mixtures and is typical for base layers placed in Italian motorways. The mixtures
117 contain 30% reclaimed asphalt pavement (RAP) by aggregate weight and their nominal maximum
118 aggregate size (NMAS) is 20 mm. The total binder content (virgin bitumen plus bitumen from
119 RAP) is 4.3% by aggregate weight for all the mixtures. The H mixture, which currently serves as
120 the reference mixture for Italian motorway pavements, was produced with SBS polymer-modified
121 bitumen with 3.8% polymer by binder weight. The GC and PC mixtures were produced using a neat
122 50/70 penetration grade bitumen and then adding the two compounds via the dry method, with a

123 dosage of 5.2% by total binder weight. The compounds, supplied in the form of hard pellets,
124 consisted of hard recycled plastic and graphene for the GC mixture and a blend of plastomeric
125 polymers for the PC mixture. The chemical characterization of the compounds carried out by
126 D'Angelo et al. [25] showed that both compounds were made mostly of polyethylene and
127 polypropylene, with the small addition of graphene for the GC mixture. **Figure 1** also reports the
128 aggregate gradation of the OG mixture with the NMAS of 14 mm. The OG mixture binder is a SBS
129 polymer-modified bitumen (3.8% polymer by binder weight) with 5.1% binder content by aggregate
130 weight. A dosage equal to 0.3% by aggregate weight of cellulose and glass fiber was added to
131 prevent drain-down issues.

Sieve (mm)	Passing (%)	
	H, GC, PC	OG
31.5	100.0	100.0
20	94.5	100.0
14	76.5	92.1
10	57.9	49.5
6.3	42.3	23.4
2	26.4	14.2
0.5	12.8	8.4
0.25	9.6	6.9
0.063	6.0	4.5

Figure 1. Aggregate gradations of investigated mixtures.

2.2. Field test track

136 A 600-m full-scale field test track was constructed in September 2020 as part of the A12 Italian
137 motorway in the city of Fiumicino and consists of milled and reconstructed asphalt layers [26]. The
138 field test track is composed of three 200-m sections, each characterized by the same pavement
139 structure, as follows:

- An open-graded wearing layer with nominal thickness of 4 cm, constructed with the OG mixture for all three sections.
- A dense-graded layer with a total nominal thickness of 25 cm, constructed with a different material for each section, i.e., the reference mixture H (representing the wet modification method), and the GC and PC mixtures modified via the dry method. The construction was carried out via the consecutive compaction of two layers: a 15-cm lower layer on the foundation, hereafter called *Field_inf*, and a 10-cm upper layer, hereafter called *Field_sup*.
- An unbound foundation layer with nominal thickness of 35 cm, placed on the subgrade.

4

2.3. Testing program and procedures

150 *2.3.1. Testing program*

151 **Figure 2** presents the testing program, which was divided into three stages. In the first stage,
152 laboratory-compacted specimens of all the study mixtures were investigated. The specimens were
153 produced using the same mixtures that were used for the field test track. The loose mixtures were
154 produced at 170°C at the asphalt plant and then sampled and immediately compacted at 160°C by a
155 gyratory compactor in accordance with EN 12697-31 [27]. As prescribed by AASHTO R 83 [28]
156 and AASHTO PP 99 [29], the gyratory-compacted samples had a diameter of 150 mm and height of
157 180 mm. Then, one large (100-mm diameter, 150-mm height) test specimen or four small (38-mm
158 diameter, 110-mm height) test specimens were vertically extracted from the inner portion of the
159 gyratory-compacted sample. Due to their high air void contents, only the large specimens were
160 considered for the OG mixture. First, given the peculiarities of the investigated materials,
161 proficiency checks were carried out by the North Carolina State University (NCSU, USA) research
162 team and the Università Politecnica delle Marche (UNIVPM, Italy) research team with the aim of
163 comparing the results for the same mixtures, H and GC, obtained from the two institutions'
164 individual laboratories. Then, all the remaining tests were carried out at the UNIVPM laboratory.
165 During the second stage of the testing program, the dense-graded cores extracted from the field test
166 track (*Field_sup* and *Field_inf*) were studied to assess the effects of *in situ* compaction. A set of
167 200-mm diameter cores was extracted from each field test section in February 2021. After cutting
168 the layers at the interface, small specimens were horizontally extracted from the *Field_sup* and
169 *Field_inf* layers [29]. The open-graded wearing layer was not included in the investigation due to its
170 limited thickness. During the first and second stages of the testing program, the fatigue behavior at
171 the material level was evaluated using the S-VECD model approach by carrying out dynamic
172 modulus tests and cyclic fatigue tests. Finally, in the third stage, the fatigue performance of the
173 mixtures was investigated at the structural level by performing FlexPAVE^{TM} pavement simulations
174 based on the laboratory test results.
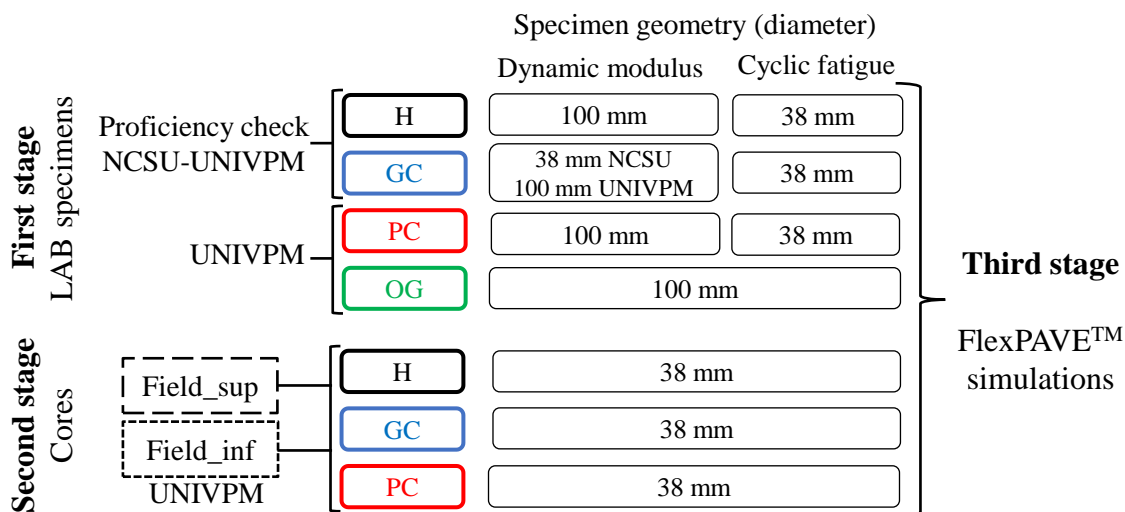
175
176 **Figure 2.** Testing program.

177

178 *2.3.2. Dynamic modulus tests*

179 Dynamic modulus tests were conducted using large specimens in accordance with AASHTO T 378
180 [30] and small specimens in accordance with AASHTO TP 132 [31] by means of an Asphalt
181 Mixture Performance Tester (AMPT). The test temperatures that were needed to obtain the
182 viscoelastic properties (dynamic modulus $|E^*|$ and phase angle δ) of the materials, i.e., 4°C, 20°C,
183 and 40°C, were selected in accordance with the reference standards [31][32]. The frequencies
184 investigated for each temperature were 0.1 Hz, 0.5 Hz, 1 Hz, 5 Hz, and 10 Hz, plus 0.01 Hz at 40°C
185 (to improve the prediction of the behavior at low reduced frequencies). The specimens were
186 subjected to sinusoidal axial compression loading; the amplitude was varied to maintain average
187 strain levels of 100 $\mu\varepsilon$ and 63 $\mu\varepsilon$ for the large and small specimens, respectively. At least two and
188 three replicate specimens were tested for each mixture for the large and small specimens,
189 respectively.

190 The mastercurves and shift factors were determined by minimizing the error between the
191 experimental data and results from the 2S2P1D model that was applied for the storage modulus (E_1
192 $= |E^*|\cdot\cos\delta$) [30][31]. Equation (1) presents the 2S2P1D model, which is represented by a
193 combination of two springs, two parabolic elements, and one dashpot.

$$E_1(i\omega\tau) = E_{1,0} + \frac{E_{1,\infty} - E_{1,0}}{1 + \delta(i\omega\tau)^{-k} + (i\omega\tau)^{-h} + (i\omega\beta\tau)^{-1}} \tag{1}$$

194 where $E_{1,0}$ and $E_{1,\infty}$ are the storage modulus values for frequency $\omega \to 0$ and $\omega \to \infty$, respectively,
195 and describe the behavior of the springs; k and h describe the behavior of the parabolic elements; δ
196 is a proportional constant between the parabolic elements; and β is linked to the Newtonian
197 viscosity of the dashpot [33].

198 *2.3.3. Cyclic fatigue tests*

199 Cyclic fatigue tests were conducted using small specimens for the three dense-graded mixtures in
200 accordance with AASHTO TP 133 [34] and large specimens for OG in accordance with AASHTO
201 T 107 [35] by means of the AMPT. Prior to fatigue testing, a dynamic modulus fingerprint test was
202 performed to analyze the specimen-to-specimen variability and calibrate the strain level needed for
203 the fatigue tests. The fingerprint test consisted of measuring the dynamic modulus in the tension
204 compression mode of loading in a strain range of 50 µε to 75 µε at the target test temperature and at
205 the frequency of 10 Hz. The ratio of the fingerprint modulus value to the reference modulus value
206 that is derived from the mastercurve is referred to as the 'dynamic modulus ratio', and its value
207 should be within the range of 0.85 to 1.15 for each specimen to limit specimen-to-specimen
208 variability.

209 Direct tension cyclic fatigue tests were conducted at the frequency of 10 Hz in actuator
210 displacement control mode of loading. The peak-to-peak on-specimen amplitude of the sinusoidal
211 strain was selected to be between 190 µε and 290 µε in order to obtain a test duration between 2000
212 and 80000 cycles. As prescribed by the reference standards, the test temperature is the average
213 temperature of the bitumen PG minus 3°C, which must not exceed 21°C. Because the expected PG
214 for the binders in this study was PG 76-16, the testing temperature was 21°C.

215 The core experimental outcome of VECD theory is represented by the pseudo stiffness (C) versus
216 damage (S) curve, referred to as the 'damage characteristic curve'. The damage characteristic curve
217 represents the relationship between the pseudo stiffness and amount of damage of a mixture and
218 describes the fatigue damage evolution within the material [17]. Equation (2) presents the power
219 function law that expresses this relationship, which represents a fundamental property of the
220 material that is independent of mode of loading, temperature, frequency, and strain level [36].
221 Therefore, a mixture can be characterized by three valid test results that show overlapping C versus
222 S curves.

$$C = 1 - C_{11} \cdot S^{C_{12}} \tag{2}$$

223 where C is pseudo stiffness; S is damage; and C_{11} and C_{12} are fitting coefficients.

224 The D^R failure criterion was applied in this study to define material failure [37]. Equation (3)
225 defines D^R as the slope of the linear relationship that passes through zero between the average
226 reduction in pseudo stiffness and the number of cycles to failure (N_f) and is a measure of the
227 material's toughness. Following AASHTO TP 133 [34], the number of cycles to failure corresponds
228 to the cycle in which the product of the peak-to-peak stress and cycle number reaches a maximum
229 value after a stable increase during cyclic loading.

$$D^R = \frac{\int_0^{N_f}(1-C)dN}{N_f} = \frac{sum(1-C)}{N_f} \tag{3}$$

230 Equation (4) defines the apparent damage capacity index, S_{app} [34][35]. This index parameter was
231 developed by Wang et al. [38] and takes into account all the properties that affect the cracking
232 potential of a mixture within the pavement, i.e., stiffness, damage tolerance, and toughness. S_{app} is
233 determined at a specific temperature that is based on the climatic PG of the location where the
234 pavement is constructed. Given that the field test track is located in a PG 58-10 climatic zone [39],
235 the S_{app} reference temperature used in this study was 21°C.

$$S_{app} = 1000^{\left(\frac{\alpha}{2}-1\right)} \cdot \frac{a_{T(Sapp)}^{\frac{1}{\alpha+1}} \cdot \left(\frac{D^R}{C_{11}}\right)^{\frac{1}{C_{12}}}}{|E^*|^{\frac{\alpha}{4}}_{LVE,Sapp}} \tag{4}$$

236 where α is the damage growth rate; $a_{T(Sapp)}$ is the time-temperature shift factor between the S_{app}
237 temperature and the reference temperature considered for the dynamic modulus mastercurve; and
238 $|E^*|^{\frac{\alpha}{4}}_{LVE,Sapp}$ is the reference modulus calculated at the S_{app} reference temperature and at the
239 reduced frequency of 62.8· $a_{T(Sapp)}$. S_{app} values usually vary within a range of 0 to 50, and higher
240 values indicate better fatigue resistance.

3. Results and analysis

3.1. Proficiency check

243 The proficiency checks, which aimed to check for the reproducibility of the tests that were
244 conducted at the NCSU and UNIVPM laboratories, involved laboratory-compacted specimens of
245 the H and GC mixtures. First, the large specimen geometry (100-mm diameter) was selected,

246 because the NMAS of the mixtures was slightly higher than 19 mm, which is the maximum NMAS
247 prescribed by the reference standards for small specimens [29][31][34]. However, to assess the
248 feasibility of using the small specimen geometry (38-mm diameter), small specimens were
249 considered for the dynamic modulus tests of the GC specimens at NCSU (see **Figure 2**). In order to
250 exclude the influence of the volumetric properties, the tested specimens had air void contents within
251 the range of 2.2% and 3.3%. The density of the specimens was measured using the automatic
252 sealing method [40] at NCSU and the saturated surface dry method [41] at UNIVPM. According to
253 AASHTO PP 99 [29], these two methods can be used indifferently for calculating the density of
254 dense-graded asphalt specimens.

255 **Figure 3** (a) and (b) respectively show the dynamic modulus mastercurves of the H and GC
256 specimens tested at NCSU and UNIVPM. The results at the reference temperature of 21.1°C (70°F)
257 overlap for both mixtures at both laboratories, demonstrating the good reproducibility and
258 repeatability of the dynamic modulus tests.


(a)　　　　　　　　　　　　　　**(b)**
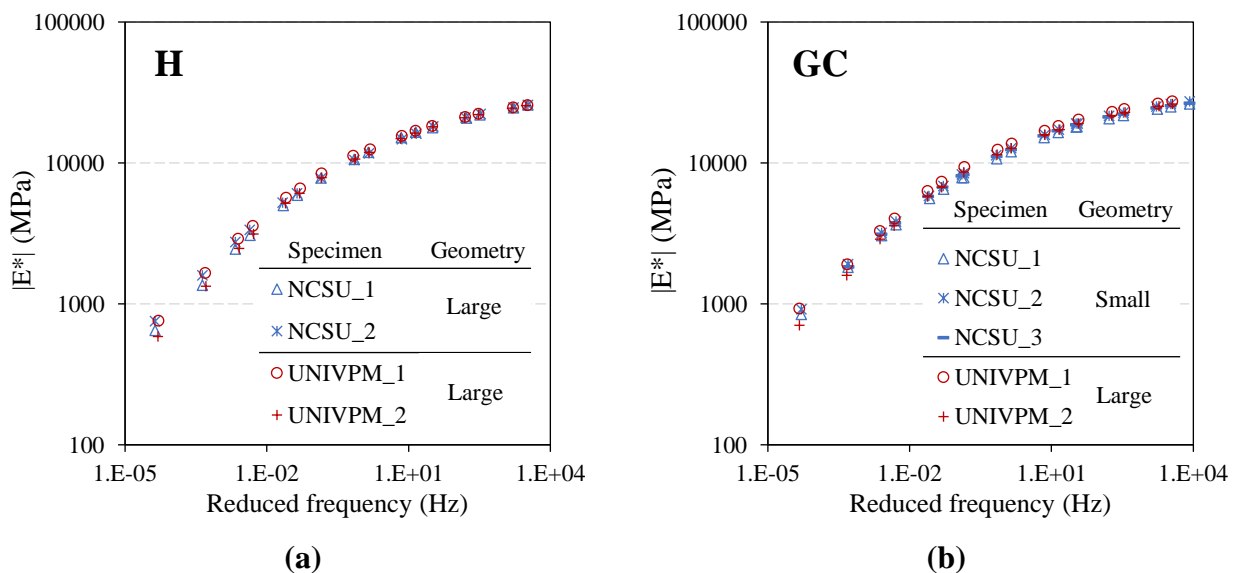
259 **Figure 3.** Proficiency check results: dynamic modulus mastercurves for individual specimens of (a)
260 mixture H and (b) mixture GC at 21.1°C.

261

262 In addition, the overlapping results of the GC mixture obtained from specimens with different
263 geometries, i.e., the large specimens tested at UNIVPM and the small specimens tested at NCSU
264 (see **Figure 2**), demonstrate that the small specimen geometry complies with the representative
265 volume element despite the NMAS of 20 mm. As a consequence, the small specimen geometry was
266 adopted for the cyclic fatigue tests.

267 **Figure 4** (a) and (b) respectively show the damage characteristic curves of H and GC obtained at
268 NCSU and UNIVPM. Considering that the damage characteristic curve is a fundamental property of
269 the material, and that it is not influenced by the testing and boundary conditions [36], the overlap of
270 the *C* versus *S* curves indicates good reproducibility and repeatability of the fatigue tests.

8

(a)   **(b)**
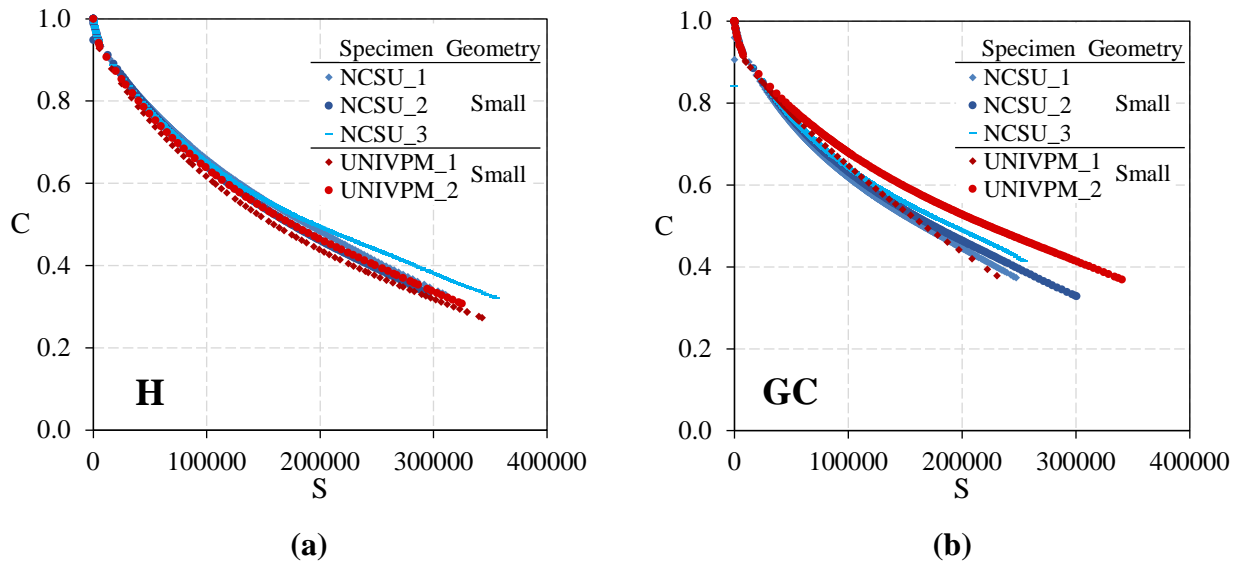
Figure 4. Proficiency check: damage characteristic curves for individual specimens of (a) mixture H and (b) mixture GC.

3.2. Laboratory specimens

As a follow-up to the successful proficiency checks, laboratory specimens PC and OG also were investigated by means of dynamic modulus and cyclic fatigue tests. The following Sections 3.2.1 and 3.2.2 present comparisons of the results obtained from the laboratory-compacted dense-graded mixtures, H, GC, and PC, and the results obtained for the open-graded mixture, OG, respectively.
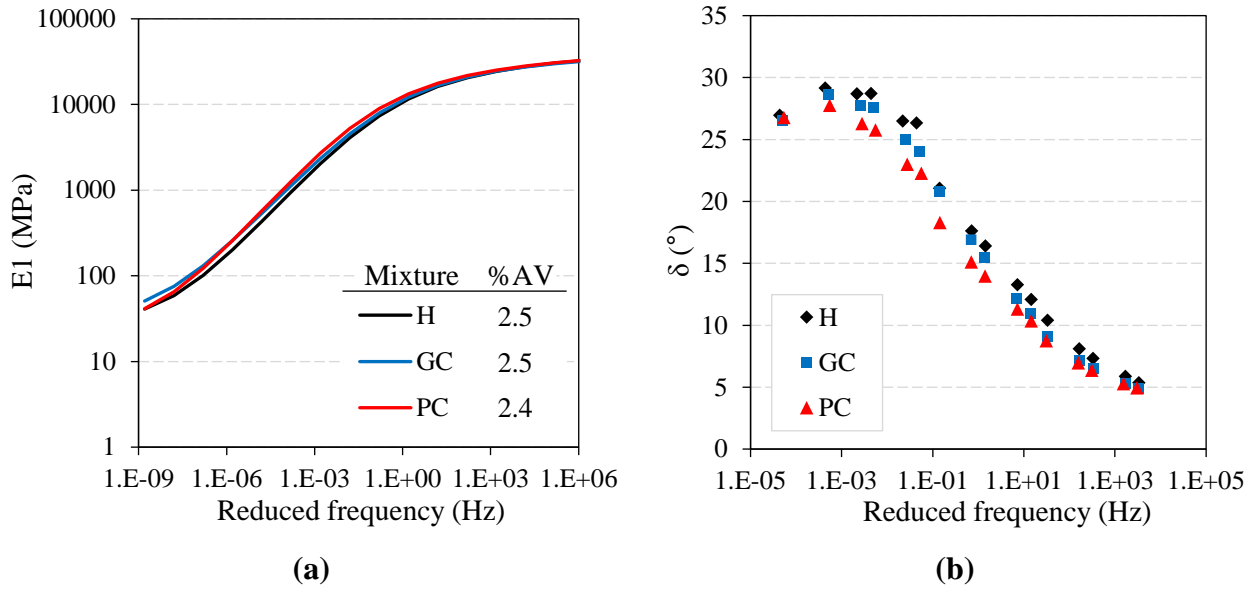
3.2.1. Dense-graded mixtures

Figure 5 (a) and (b) respectively show the storage modulus mastercurves based on the 2S2P1D model and the phase angle mastercurves at the reference temperature of 21.1°C for all the dense-graded mixtures. Obviously, the 2S2P1D model predictions would be less accurate for very low and very high reduced frequencies, i.e., for conditions that are significantly different from those investigated in the laboratory (approximately between 10^{-5} Hz and 10^4 Hz). Note that the H, GC, and PC mixtures were characterized by the same volumetric properties.

Figure 5 (**a**) shows that the dynamic modulus mastercurves basically overlap, meaning that H, GC, and PC have comparable stiffness values overall. This result confirms the findings by Cardone et al. [26], who observed that, under the same volumetric properties, the mixtures present similar indirect tensile stiffness modulus values (EN 12697-26) [42] when measured at 20°C and 2 Hz. Specifically, H exhibits a slightly lower stiffness value within a wide range of reduced frequencies compared to the mixtures modified by the dry method, whereas the PC and GC curves have slightly different dynamic modulus mastercurve shapes. **Figure 5** (a) also reports the average air void contents ('%AV') of each mixture, calculated using the saturated surface dry method.

The phase angle mastercurves presented in **Figure 5 (b)** confirm that the mixtures modified by the dry method (especially PC) are more elastic and less viscous than the reference mixture H, as denoted by their lower phase angle values. Even at the binder level, D'Angelo et al. [25] observed a

9

297 predominance of the elastic component of the dynamic modulus for the GC and PC binders
298 compared to the H binder, especially at high temperatures. Moreover, lower phase angle values can
299 be observed for the binders modified with the compounds compared to the polymer-modified
300 bitumen [25].

(a)

(b)

301 **Figure 5.** Laboratory specimens, dense-graded mixtures: (a) storage modulus mastercurves
302 (2S2P1D model) and (b) phase angle mastercurves at 21.1°C.

303

304 **Figure 6** (**a**) shows the fit of the C versus S curves for each mixture obtained from three replicate
305 overlapping curves. The figure also reports the average air void contents of the specimens
306 investigated in the fatigue tests. Note that these average air void contents are close to those of the
307 specimens used in the dynamic modulus tests; see **Figure 5 (a)**. The curves are similar for all the
308 dense-graded mixtures, which is probably due to their comparable stiffness values, also shown in
309 **Figure 5**. Nevertheless, H and PC reached lower pseudo stiffness values at failure compared to GC,
310 suggesting their greater capacity to tolerate damage. It is underlined that the fatigue resistance of the
311 mixture cannot be evaluated solely based on the position of the damage characteristic curve (which
312 mainly depends on the mixture's stiffness). The damage characteristics provided by the C versus S
313 curve should be always combined with the mixture's toughness, quantified by the D^R value. This is
314 possible thanks to the S_{app} parameter (Equation (4)), which allows to predict the fatigue
315 performance of the mixture within the pavement.

316 **Figure 6** (**b**) shows the results based on the failure criterion D^R, which is the slope of the linear
317 relationship presented in Equation (3). The dense-graded mixtures basically are characterized by
318 similar values. However, the slightly higher value observed for H (i.e., 0.496) indicates its greater
319 ability to absorb energy before failure compared to GC and PC. This outcome could be ascribed to
320 the different binder phases of the mixtures, i.e., the polymer-modified bitumen for mixture H versus
321 the neat bitumen for mixtures GC and PC.

(a)   **(b)**
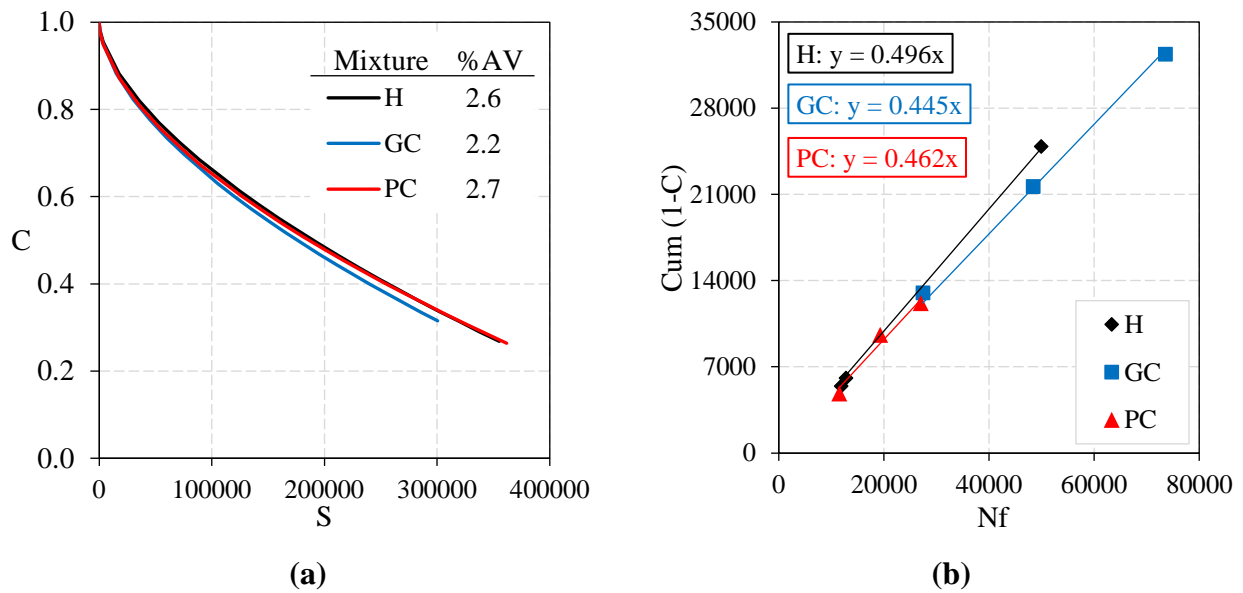
322   **Figure 6.** Laboratory specimens, dense-graded mixtures: (a) fit of damage characteristic curves and
323   (b) D^R failure criterion.

324   **Figure 7** presents the S_{app} values and average air void contents obtained from the dynamic modulus
325   and fatigue tests of the three dense-graded mixtures, which confirmed the rankings given by the D^R
326   values. H is characterized by the highest value followed by PC and GC, suggesting that the fatigue
327   resistance of the reference mixture is slightly better than that of the mixtures modified by the dry
328   method.

329
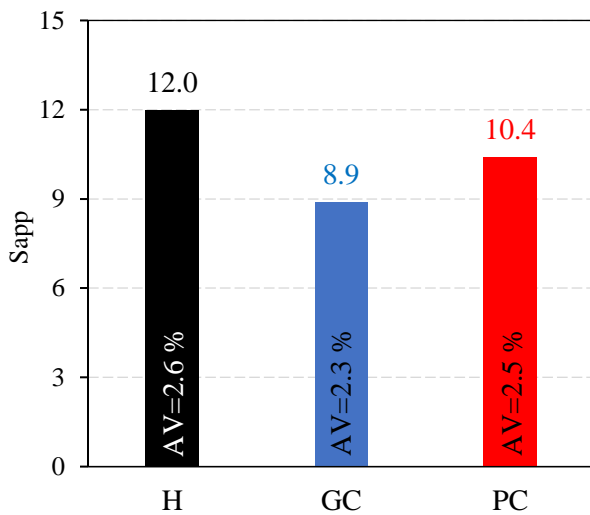
330   **Figure 7.** Laboratory specimens, dense-graded mixtures: S_{app} values.

331

332   *3.2.2. Open-graded mixture*

333   As mentioned, the open-graded mixture OG also was investigated through dynamic modulus and
334   cyclic fatigue tests (see **Figure 2**). The S-VECD model and the related transfer functions have been
335   mainly calibrated for dense-graded mixtures. Moreover, the service life of open-graded wearing
336   layers mainly depends on functional aspects, as they are usually replaced due to ravelling and/or

11

337 clogging. However, the determination of the viscoelastic and damage properties of the OG mixture
338 was necessary in order to run FlexPAVE^{TM} simulations for the study pavement that includes the OG
339 mixture as the wearing layer.

340 **Figure 8 (a)** shows the OG storage modulus mastercurve based on the 2S2P1D model at the
341 reference temperature of 21.1°C. **Figure 8 (b)** shows the fit of the OG damage characteristic curve
342 obtained from four replicate overlapping *C* versus *S* curves. These two figures also report the
343 average air void contents of the tested OG specimens, calculated using the geometric method [41].

(a)   (b)
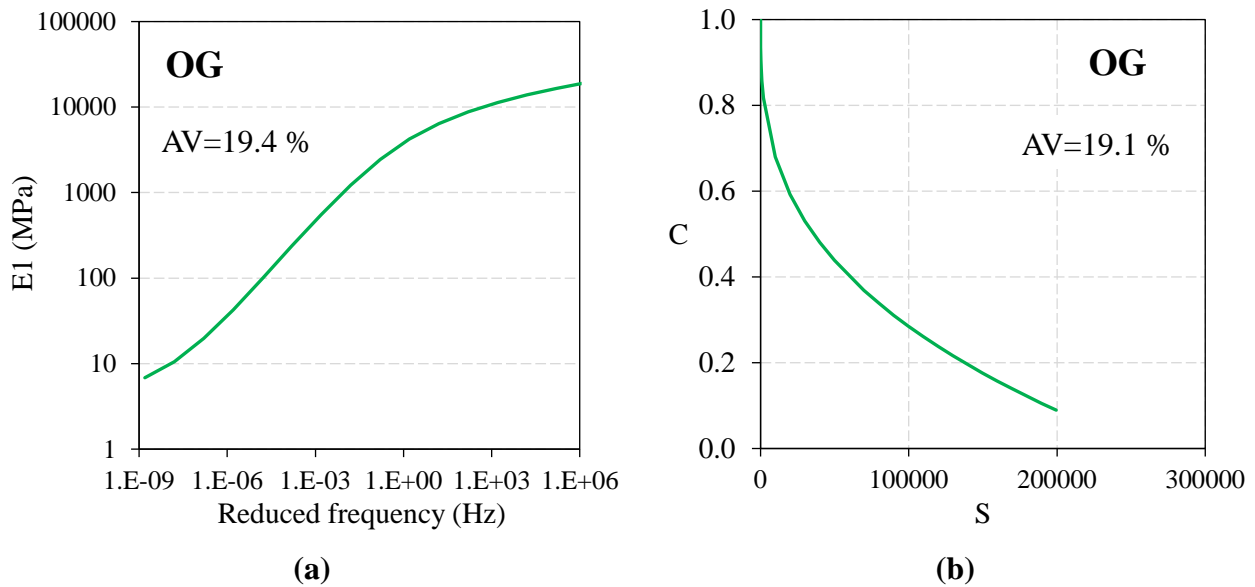
344 **Figure 8.** Mixture OG: (a) storage modulus mastercurve (2S2P1D model) at 21.1°C and (b) fit of
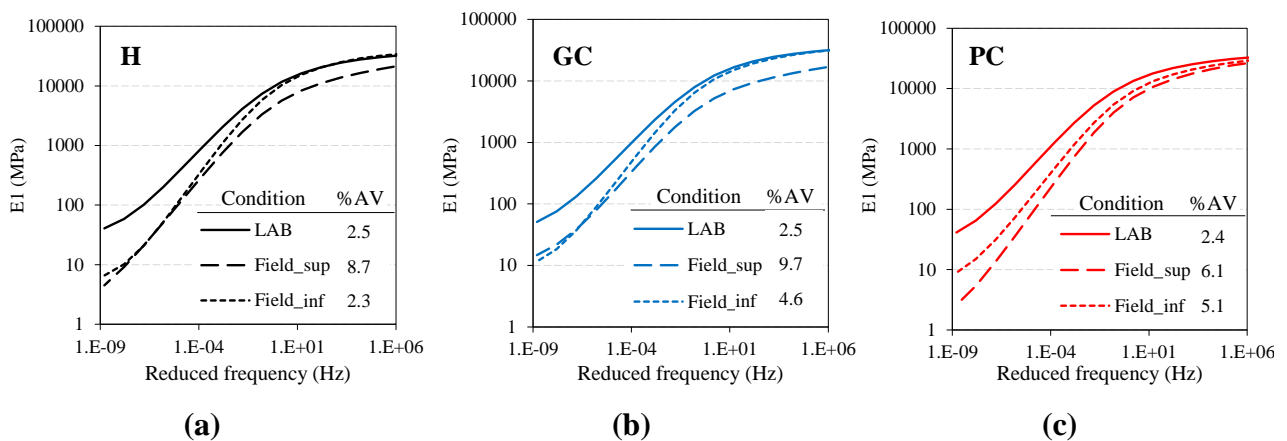345 damage characteristic curve.

346

347 ### 3.3. Field specimens

348 **Figure 9** (a), (b), and (c) present comparisons of the storage modulus mastercurves for the field and
349 laboratory specimens for each of the three mixtures, respectively, obtained based on the 2S2P1D
350 model at the reference temperature of 21.1°C. The figures also report the average air void contents
351 for each mixture.

352 Note that, in the case of the *Field_inf* layer, the air void content is comparable to that of the
353 laboratory specimens only for H, whereas both GC and PC show higher air void contents for the
354 field specimens. Moreover, for all the mixtures, the air void content of the *Field_sup* layer is higher
355 than that of the *Field_inf* layer and significantly higher than that of the laboratory specimens. As
356 discussed in depth by Cardone et al. [26], the *Field_inf* layer of mixture H underwent additional
357 compaction when *Field_sup* was constructed over it, whereas the workability of the GC and PC
358 mixtures was diminished by the presence of the compounds, whose melting points are comparable
359 to the compaction temperature (i.e., 160°C). Therefore, unlike the laboratory specimens
360 (characterized by similar volumetric properties for all mixtures), the effect of the different air void
361 contents must be considered when analyzing the behavior of field specimens.

362 **Figure 9** (a), (b), and (c) also show that all the mixtures exhibit a similar trend whereby the stiffness
363 values of the laboratory specimens are higher than those of the *Field_sup* specimens, whereas the
364 *Field_inf* specimens exhibit an intermediate stiffness value. The lowest stiffness value of the
365 *Field_sup* specimens is due to the high air void content observed for all the mixtures. Regarding the
366 *Field_inf* results, the dynamic modulus values are comparable to those of the laboratory specimens
367 at high reduced frequencies and comparable to those of the *Field_sup* specimens at low reduced
368 frequencies (even though the 2S2P1D model predictions could be less accurate at particularly low
369 and high reduced frequencies). These findings indicate a faster transition from predominantly
370 elastic behavior to predominantly viscous behavior. Moreover, recall that the dynamic modulus
371 tests were conducted using large specimens under laboratory conditions and small specimens under
372 field conditions. Therefore, the test geometry might emphasize the difference at low frequencies
373 [43].

374 Different from the compound-modified mixtures, GC and PC, the intermediate stiffness values of
375 the *Field_inf* specimens for the H mixture with SBS-modified bitumen could not be justified by the
376 intermediate air void contents, because the laboratory and *Field_inf* specimens had similar air void
377 contents of around 2.5%; see **Figure 9 (a)**. As a possible explanation, the mixtures were compacted
378 by a gyratory compactor at a fixed height (180 mm) in the laboratory, whereas the lower 15-cm
379 layer reached this compaction level in the field gradually thanks to the progressive passage of
380 rollers on the pavement. The two compaction methods can imply different compaction energy and
381 lead to different aggregate packing. In addition, the laboratory specimens were cored vertically
382 from the gyratory-compacted samples, whereas the field specimens were cored horizontally within
383 the layer (i.e., different orientation of the principal stresses).


(a) (b) (c)

384 **Figure 9.** Field vs. laboratory specimens: storage modulus mastercurves (2S2P1D model) of (a) H,
385 (b) GC, and (c) PC at 21.1°C.

386

387 **Figure 10** (a), (b), and (c) present comparisons of the fit of the damage characteristic curves
388 obtained from the *Field_sup* and *Field_inf* specimens and from the laboratory specimens for each of
389 the three mixtures, respectively. The figures also report the average air void contents of the
390 specimens subjected to fatigue tests, which are comparable to the air void contents of the dynamic
391 modulus specimens shown in **Figure 9**. **Figure 10** shows that, for all three dense-graded mixtures,
392 the curve of the laboratory specimens is in the highest position, followed by that of *Field_inf* and

13

393   then *Field_sup*. These results are consistent with the stiffness properties and air void contents (in
394   general, the curve of softer mixtures tends to stay below that of stiffer mixtures). Regarding mixture
395   H, note that the LAB curve is above the *Field_inf* curve despite their similar air void contents,
396   confirming that C versus S curves are dependent on the stiffness property, which in turn is affected
397   by the compaction and coring conditions, as mentioned earlier.

398   The H and GC field specimens reached lower C values at failure than the laboratory specimens,
399   suggesting the field specimens' greater tolerance to damage, which could be ascribed to the different
400   volumetric properties and/or compaction method (whose effects are discussed above). Moreover, the
401   high value of S at failure observed for H in the *Field_inf* condition suggests that this mixture is able
402   to tolerate a greater amount of damage compared to all the other investigated mixtures. However,
403   recall that the C versus S curve alone does not provide complete information on the fatigue resistance
404   and thus should be always combined with D^R into the S_{app} value. The curve of *Field_sup* for the GC
405   mixture, which is characterized by the C value at failure that is close to 0, is considered unreliable
406   due to the high air void content (i.e., 10%), which could lead to problems related to the
407   representativeness of the small specimen geometry. Conversely, for PC, all the curves can be
408   characterized by similar pseudo stiffness values at failure.

(a)   (b)   (c)
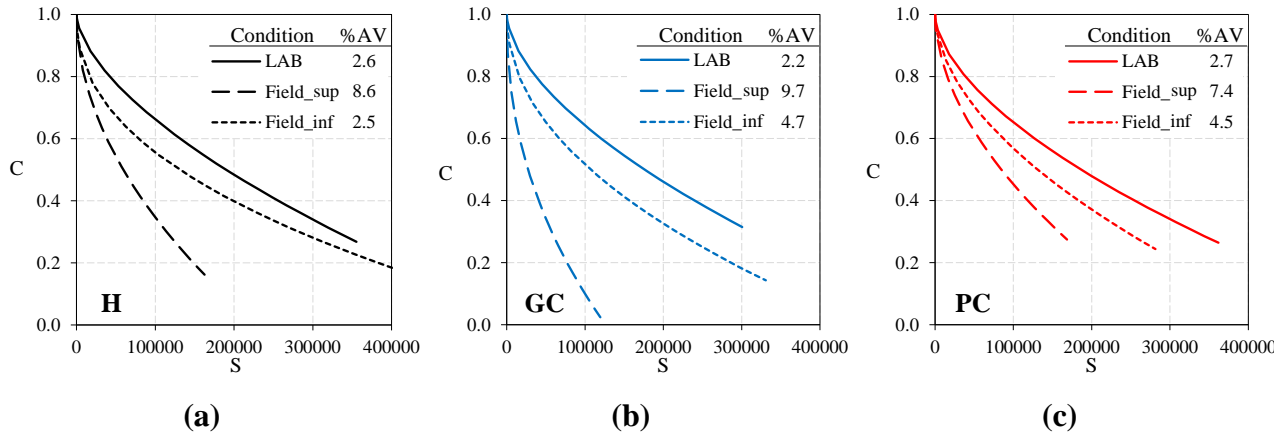
409   **Figure 10.** Field vs. laboratory specimens: fit of damage characteristic curves for (a) H, (b) GC, and
410   (c) PC.

411

412   **Table 1** presents the D^R values for all the mixtures. The toughness, i.e., the ability to absorb energy
413   before fracture, of the field specimens is always significantly greater than that of the laboratory
414   specimens, suggesting that the laboratory compaction process leads to a reduction in toughness (i.e.,
415   possible over-compaction causing some broken aggregate, especially within the RAP fraction). The
416   extremely high D^R value (0.876) observed for *Field_sup* of GC confirms the unrealistic results for
417   this mixture. No clear trend related to air void content was observed in terms of D^R.

418   **Table 1.** Field vs. Laboratory Specimens: D^R Values

Condition	H	GC	PC
Laboratory	0.496	0.445	0.462
Field_sup	0.619	0.876	0.481
Field_inf	0.610	0.581	0.514

14

419

The S_{app} values in **Figure 11** (a), (b), and (c) confirm the findings from the damage characteristic
curves and D^R failure criterion for the three mixtures. The figures also report the average air void
contents of all the specimens used for the dynamic modulus and fatigue tests. Better fatigue
resistance can be expected from the field specimens, especially from *Field_inf* specimens, which
are characterized by an intermediate stiffness value that ensures good distribution of the stress
within the pavement without compromising the mixture's toughness. The highest S_{app} value of 22.4,
observed for H in the *Field_inf* condition, can be associated with the high S value at failure
observed for this mixture; see **Figure 10 (a)**.
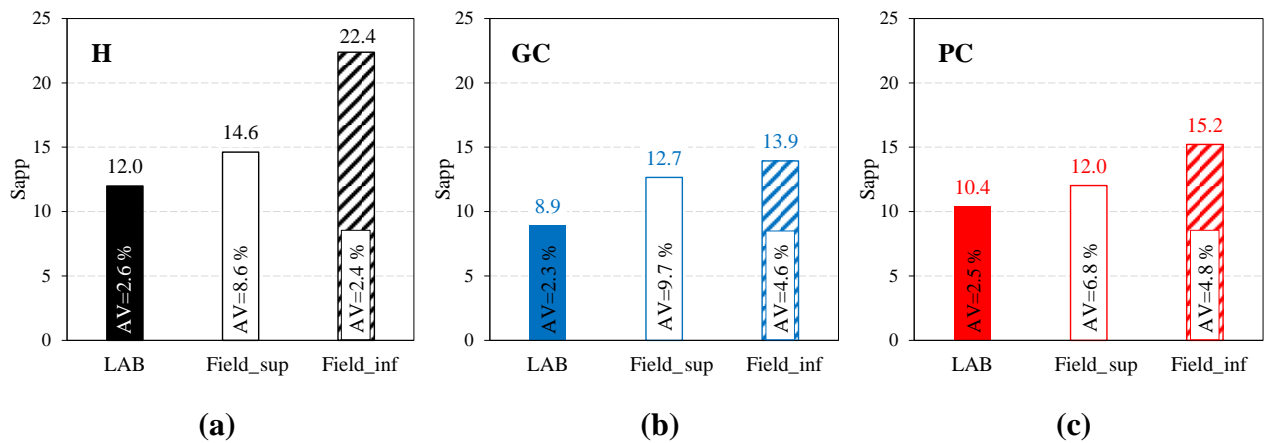
Figure 11. Field vs. laboratory specimens: S_{app} values for (a) H, (b) GC, and (c) PC.

Overall, based on the analysis of the mixtures at the material level, the compound-modified
mixtures, GC and PC, show similar performance, which is slightly worse than the performance of
the reference mixture, H. These results are in agreement with those obtained by Cardone et al. [26]
through indirect tensile fatigue tests (EN 12697-24) [44]. Moreover, the analysis results indicate
that an intermediate material stiffness value can lead to better fatigue resistance of the pavement, as
expressed by the S_{app} parameter.

4. Pavement performance simulations

Pavement performance simulations were carried out using FlexPAVE[TM], which takes into account
both the moving nature of traffic loads and climatic conditions that affect the pavement [23][24].
Using FlexPAVE[TM], the pavement is modeled as a three-dimensional layered viscoelastic structure,
and the finite element method with Fourier transform is embedded to predict long-term mechanical
responses [45].

The spatial distribution response of the damage factor was analyzed in this study. The damage
factor is defined as the ratio of the current number of cycles (N) to the number of cycles at failure
(N_f). The damage factor ranges from 0 to 1, with 1 indicating an asphalt element that is completely
cracked. Moreover, the time history (or evolution) of the percentage of damage, defined as the ratio
of the sum of the damage factors within the cross-section area to the total area, also was evaluated
in this study. Equation (5) defines the percentage of damage *(%Damage)*. Specifically,
FlexPAVE[TM] calculates the *%Damage* based on a reference cross-section area affected by stresses
and strains due to traffic loading [23].

15

$$\%Damage = \frac{\sum_{i=1}^{M}(N/N_f)_i \cdot A_i}{\sum_{i=1}^{M} A_i} \tag{5}$$

449 where i is the nodal point number in the finite element mesh; M is the total number of nodal points
450 in the finite element mesh; and A_i is the area that corresponds to the nodal point i in the finite
451 element mesh.

452 Equation (6) presents the sigmoidal transfer function proposed by Wang et al. [24] that was used to
453 create a relationship between the *%Damage* in the cross-section provided by FlexPAVE™ and the
454 percentage of cracking (*%Cracking*) on the surface of the pavement.

$$\%Cracking = \frac{50}{1 + C_{f1} \cdot \exp\left[C_{f2} \cdot \left(\log C_{f3} - \log \%Damage\right)\right]} \tag{6}$$

455 where 50 is the maximum *%Cracking*; and C_{f1}, C_{f2}, and C_{f3} are calibration factors whose values
456 are 0.342, 13.97, and 16.38, respectively.

4.1. Input data

458 In this study, FlexPAVE™ analysis was performed for a 30-year pavement service life under both
459 thermal effects and traffic loading. The structure of the simulated pavement is the same as the
460 Fiumicino field test track and consists of a 4-cm open-graded wearing layer, a 25-cm dense-graded
461 asphalt layer, and a 35-cm foundation on the subgrade. **Table 2** presents a summary of the three
462 scenarios evaluated in the simulations. For all three scenarios, the upper 4-cm layer is modeled
463 based on the OG results, whereas the material properties of the 25-cm layer used as input differ.
464 Note that, in the context of FlexPAVE™ simulations, a 25-cm layer is equivalent to two separate
465 layers of 10 cm (*Field_sup*) and 15 cm (*Field_inf*) with the same properties, presenting perfect
466 bonding at the interface, as preliminarily verified in this study. The decision to consider a single
467 layer with 25-cm thickness was based on the fact that it requires less computational time. In
468 Scenario 1, the dense-graded layer was modeled using the results of the laboratory specimens. In
469 Scenario 2 and Scenario 3, the dense-graded layer was modeled using the results of *Field_sup*
470 (excluding GC for the reasons mentioned in Section 3.3) and *Field_inf* specimens, respectively. The
471 foundation and the subgrade were modeled as linear elastic materials with stiffness modulus values
472 of 400 MPa and 150 MPa, respectively, determined from FWD tests [26].

473 **Table 2.** Pavement Performance Simulations: Material Properties Considered for Each Scenario

Scenario	Wearing layer (4 cm)	Dense-graded layer (25 cm)	Foundation (35 cm)	Subgrade
1	OG	LAB (H, GC, PC)	$E = 400$ MPa	$E = 150$ MPa
2	OG	*Field_sup* (H, PC)	$E = 400$ MPa	$E = 150$ MPa
3	OG	*Field_inf* (H, GC, PC)	$E = 400$ MPa	$E = 150$ MPa

474

475 As for the climatic conditions, based on a comparison of the annual temperatures and precipitation,
476 the Italian city of Fiumicino (where the field test track is located) best matches San Luis Obispo in

477 California (whose climatic data are present in the FlexPAVE^{TM} database). Regarding the loading
478 conditions, as revealed from traffic data studies conducted in 2019, the field test track is subjected
479 to one million equivalent standard axle loads (ESALs) per year, where the reference ESAL is a 120-
480 kN single axle with dual wheels. In order to assess the damage caused by motorway heavy traffic, a
481 speed of 90 km/h and a tire inflation pressure of 800 kPa were considered. The tire-pavement
482 contact area was set as circular, and linear traffic growth of 0.4% per year was estimated.

4.2. FlexPAVE^{TM} results

484 **Figure 12** (a), (b), and (c) present the damage contours of H, GC, and PC, respectively, for
485 Scenario 1 (i.e., with the material properties of the laboratory specimens for the dense-graded
486 asphalt layer; see **Table 2**) after 30 years of service. Recall that the H, GC, and PC laboratory
487 specimens present analogous volumetric properties, i.e., air void contents around 2.5%, as reported
488 also in **Figure 12**. **Figure 12** clearly indicates that the damage is concentrated mainly in the upper
489 part of the asphalt layers, in particular under the 4-cm wearing layer. This damage distribution is
490 likely attributable to the thermal effects that are due to the difference in stiffness values between the
491 open-graded and dense-graded layers. Note, too, that thermal loading is similar to the loading
492 applied in a displacement-controlled test, and the resistance of the mixture to thermal loading
493 depends on the mixture's capacity to relieve the stress and resist the damage that is due to the
494 induced stress [22]. Mixture H is less prone to thermal damage than GC and PC, because the latter
495 mixtures are slightly stiffer and more brittle (i.e., greater induced stress and lower tolerance to
496 damage) and have lower phase angle values (i.e., less capacity to relieve stress) than H (**Figure 5**).
497 Bottom-up cracking, which relates strictly to fatigue stress, is limited in all the cases because of the
498 significant stiffness of the laboratory specimens (**Figure 5**), which determined the low tensile strain
499 at the bottom of the asphalt layers.

(a)   (b)   (c)
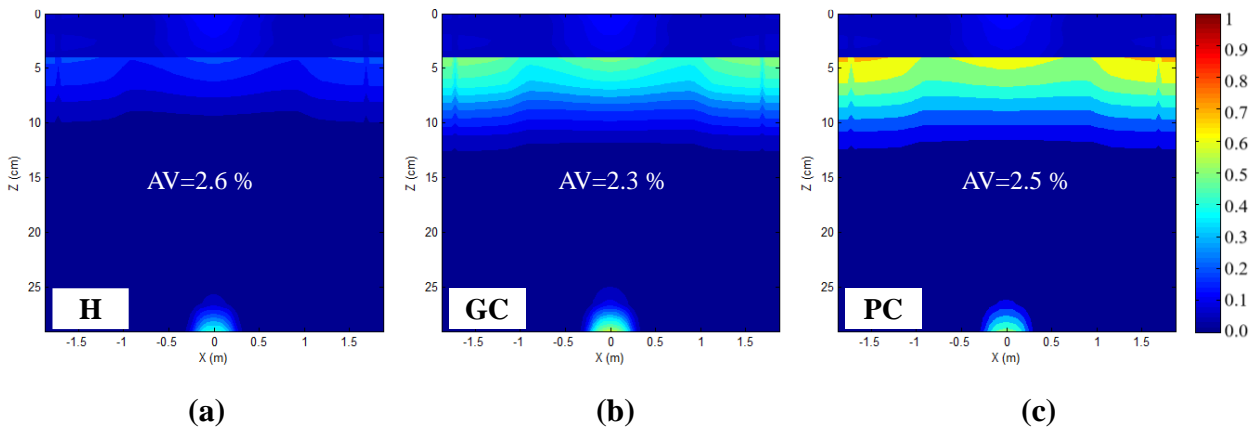
500 **Figure 12.** Scenario 1: Damage contours of **(a)** H, **(b)** GC, and **(c)** PC after 30 years.
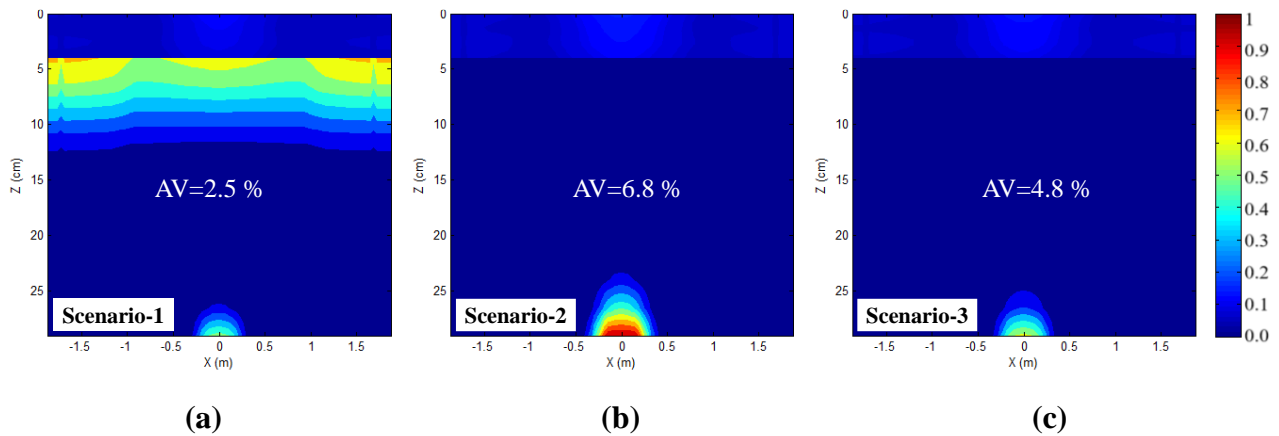
501

502 **Figure 13** (a) illustrates the Scenario 1 damage evolution within the pavement during the 30 years
503 of service, whereas **Figure 13** (b) reports the percentage of damage and the percentage of cracking
504 after the 30 years of service. Percent of damage at the end of 30 years for H, GC, and PC is 7.0,
505 14.1 and 18.0%, respectively. After applying the transfer function in Equation (6), the percentage of
506 cracking is 0.8%, 27.2%, and 41.9% for H, GC, and PC, respectively. The ratios of *%Damage* and
507 *%Cracking* between GC and PC are about the same. However, *%Cracking* of H is much smaller

17

508   than the *%Damage*. In fact, according to the considered transfer function, when *%Damage* is lower
509   than 10%, the corresponding *%Cracking* increases slowly and usually remains lower than 5%.
510   Instead, when *%Damage* is higher than 10%, *%Cracking* increases dramatically [24]. The reason is
511   that *%Damage* is calculated from the pavement cross-section whereas *%Cracking* is measured from
512   pavement surface. That is, fatigue cracking cannot be seen on the pavement surface while fatigue
513   damage grows within the asphalt layer. Overall, the better performance of H can be attributed to its
514   polymer-modified bitumen.
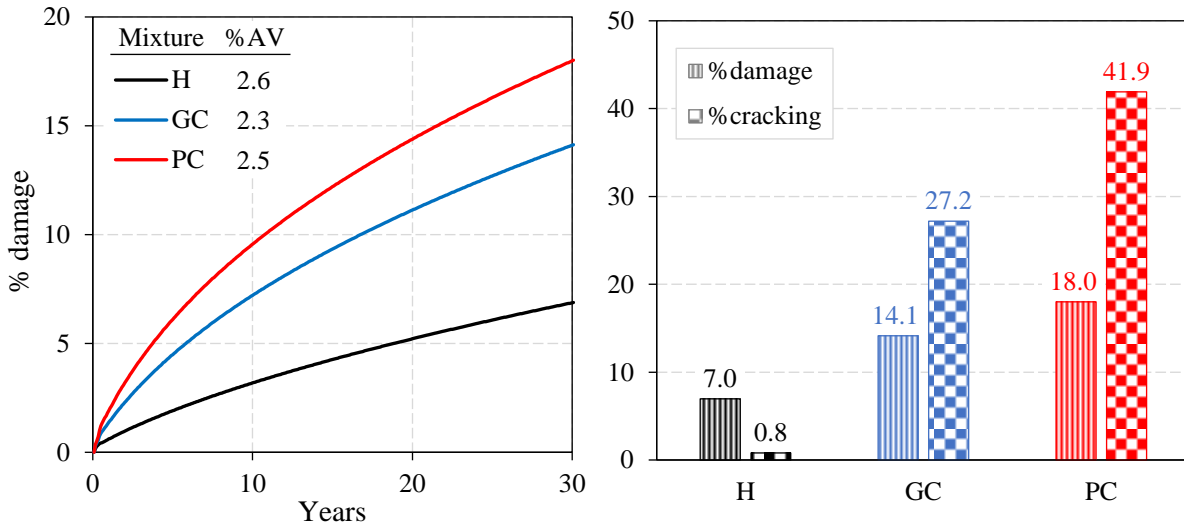
516   **Figure 13.** Scenario 1: **(a)** damage evolution, and **(b)** percentages of damage and cracking after 30
517   years.

519   **Figure 14** (a), (b), and (c) respectively present the damage contours for the PC mixture in Scenario
520   1 (laboratory specimens), Scenario 2 (*Field_sup* specimens), and Scenario 3 (*Field_inf* specimens)
521   after 30 years of service, together with the average air void contents of the specimens. As stated
522   earlier, in Scenario 1, the damage involves a large area under the wearing layer due to the difference
523   in stiffness values between the layers, which led to significant thermal damage in this study. In
524   Scenario 2, the damage is shown to be concentrated mostly at the bottom of the asphalt layer (i.e.,
525   bottom-up cracking), even though the involved area is only 6 cm to 7 cm thick. This behavior is due
526   to the lower stiffness values of the *Field_sup* specimens compared to the laboratory specimens
527   (**Figure 9**) and relates strictly to the higher air void content. Finally, in Scenario 3, an intermediate
528   behavior (that falls between the other two scenarios) can be observed whereby the pavement is
529   subjected to limited damage at the bottom of the asphalt layer (bottom-up cracking) and the upper
530   part of the asphalt layer (top-down cracking). However, the damage level observed for the open-
531   graded wearing layer might not be fully reliable due to the limited data available in the literature
532   regarding the S-VECD model characterization of open-graded mixtures (as anticipated in Section
533   3.2.2). These findings suggest that the best performance at the structural level can be expected from
534   dense-graded mixtures characterized by an intermediate stiffness level, which ensures a limited
535   stress-strain level within the pavement without negatively affecting the mixture's toughness and
536   thermal resistance. Similar observations could be made for H and GC, and thus, the results for H
537   and GC are not shown here for brevity.

(a)   **(b)**   **(c)**

Figure 14. Damage contours for PC mixture: (a) Scenario 1, (b) Scenario 2, and (c) Scenario 3.

Figure 15 (a) shows the damage evolution within the pavement during 30 years of service for the PC mixture, whereas **Figure 15** (b) reports the percentage of damage and the percentage of cracking after the 30 years of service for each Scenario. For the specimens obtained from the field test track, the percentage of damage after 30 years reached between 5% and 10%, corresponding to a very low percentage of surface cracking (lower than 3.2%), as explained earlier. A comparison of **Figure 14** and **Figure 15** shows that the wide difference in the percentage of cracking between the LAB and field conditions can be ascribed to the damage that is due to thermal stress. Given that only mixture H did not suffer thermal damage (see **Figure 12**), the viscoelastic properties derived from the modification of the binder can reasonably be assumed to provide beneficial effects, which are not provided through the dry modification of neat bitumen.
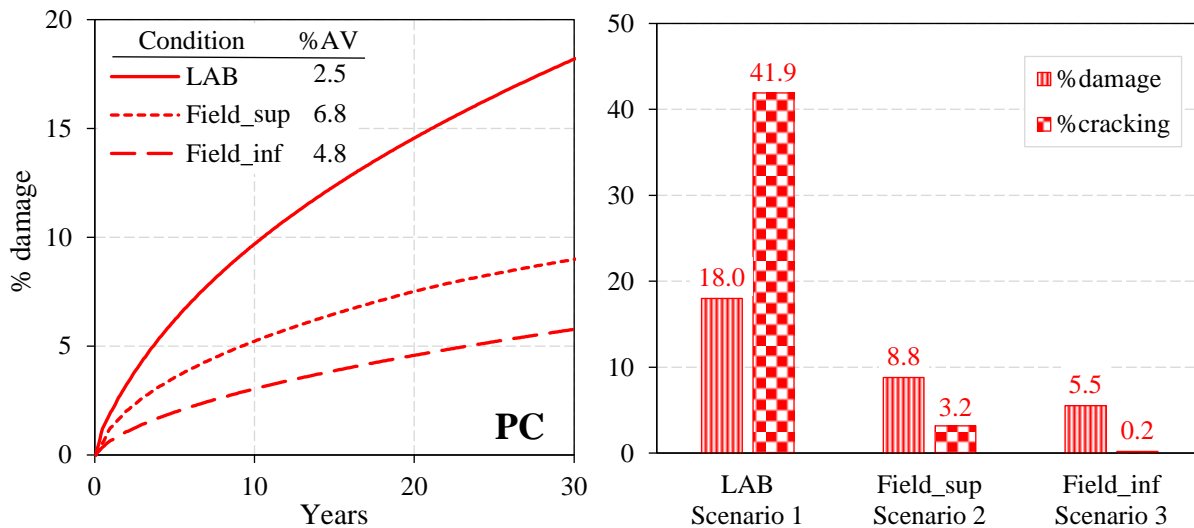
Figure 15. PC mixture: **(a)** damage evolution, and **(b)** percentages of damage and cracking after 30 years under the three scenarios considered.

5. Conclusions

This study aimed to compare the fatigue performance of a reference mixture (H) that contains bitumen modified via the wet method and two compound mixtures (GC and PC) modified via the dry method. The two compounds basically consist of polyethylene and polypropylene, plus graphene for GC. The analysis was conducted by applying the S-VECD modeling approach, which

19

includes dynamic modulus tests and direct tension cyclic fatigue tests whose results were used as input for FlexPAVE™ pavement performance simulations. The mixtures were produced at an asphalt plant and were used to construct a 25-cm base layer (placed and compacted in two separate steps, 15 cm + 10 cm) in a field test track as part of an Italian motorway. Part of the mixtures also were compacted in the laboratory.

This study demonstrates for the first time the applicability of the S-VECD modeling approach also to non-conventional materials such as asphalt mixtures modified with plastics via the dry method. The main strength of this approach is that it allows to determine fundamental fatigue properties of the material, which are independent of the testing conditions, and to predict the long-term fatigue performance of the pavement (unlike the conventional empirical fatigue tests, whose results are valid only under the specific boundary and loading conditions considered).

Under the same volumetric properties, the investigated mixtures show comparable stiffness values and fatigue resistance overall, even though the mixtures with the compounds are slightly stiffer and less viscous than the reference mixture. However, based on the FlexPAVE™ simulations, the mixtures with the compounds are much more prone to thermal damage compared to the reference mixture. This outcome is due mainly to the greater difference in stiffness values with the open-graded wearing layer. Compared to the laboratory specimens, the field specimens can be characterized by less stiffness as a consequence of their higher air void contents and different compaction conditions. In particular, the intermediate stiffness level, which characterizes the *Field_inf* specimens of all the mixtures, correlates with several positive effects: greater damage tolerance and toughness at the material level and less thermal damage and limited bottom-up cracking at the structural level.

Taking into account also the workability issues of GC and PC that are related to the melting point of plastics, the findings suggest that the performance of the reference mixture with the polymer-modified bitumen (H) is slightly better than the performance of the mixtures modified using the dry method (GC and PC). However, the addition of the polymeric compounds certainly improves the performance of mixtures with neat bitumen, even though graphene does not seem to add any positive contribution. Moreover, the environmental benefits generated from the dry modification method, i.e., reduced operational effort and the possibility of recycling waste plastics, also should be taken into consideration. Monitoring the existing motorway field test track over time will provide further data regarding the behavior of the mixtures in the field.

Author contributions

Conceptualization: Francesco Canestrari

Methodology: Francesco Canestrari, Y. Richard Kim, Lorenzo Paolo Ingrassia, Sara Spadoni

Project administration: Francesco Canestrari

Investigation: Sara Spadoni, Lorenzo Paolo Ingrassia, Douglas Mocelin

Formal analysis: Francesco Canestrari, Y. Richard Kim, Lorenzo Paolo Ingrassia, Sara Spadoni, Douglas Mocelin

596 Writing – original draft: Sara Spadoni, Lorenzo Paolo Ingrassia

597 Writing – review and editing: Francesco Canestrari, Y. Richard Kim, Douglas Mocelin.

598

Declaration of Competing Interest

600 The authors declare that they have no known competing financial interests or personal relationships
601 that could influence the work reported in this paper.

602

Acknowledgments

607

Data Availability Statement

609 The datasets generated and/or analyzed during this study are available from the corresponding
610 author upon reasonable request.

611

Funding

References

   [1] Burak S, Isikyakar G. Evaluation of the properties and microstructure of SBS and EVA polymer-modified bitumen. *Construction and Building Materials*. 2008; 22(9): 1897–1905. doi:10.1016/j.conbuildmat.2007.07.013

   [2] Mazumder M, Kim H, Lee SJ. Performance properties of polymer-modified asphalt binders containing wax additives. *International Journal of Pavement Research and Technology*. 2016; 9(2): 128-139. doi:10.1016/j.ijprt.2016.03.004

   [3] Airey GD. Styrene butadiene styrene polymer modification of road bitumens. *Journal of Materials Science*. 2004; 39(3): 951-959. doi:10.1023/B:JMSC.0000012927.00747.83

   [4] Lin P, Yan C, Huang W, Li Y, Zhou L, Tang N, Xiao F, Zhang Y, Lv Q. Rheological, chemical and aging characteristics of high content polymer-modified asphalt. *Construction and Building Materials*. 2019; 207: 616-629. doi:10.1016/j.conbuildmat.2019.02.086

   [5] Willis R, Yin F, Moraes R. *Recycled Plastics in Asphalt Part A: State of Knowledge*. National Asphalt Pavement Association. 2020; IS-142.

   [6] Wu S, Montalvo L. Repurposing waste plastics into cleaner asphalt pavement materials: A critical literature review. *Journal of Cleaner Production*. 2021; 280: 124355. doi:10.1016/j.jclepro.2020.124355

   [7] Zani L, Giustozzi F, Harvey J. Effect of storage stability on chemical and rheological properties of polymer-modified asphalt binders for road pavement construction. *Construction and Building Materials*. 2017; 145: 326-335. doi:10.1016/j.conbuildmat.2017.04.014

   [8] Ranieri M, Costa L, M. Oliveira Jr., R. D. Silva HM, Celauro C. Asphalt surface mixtures with improved performance using waste polymers via dry and wet processes. *Journal of Materials in Civil Engineering*. 2017; 29(10): 04017169. doi:10.1061/(ASCE)MT.1943-5533.0002022

   [9] Chavez F, Marcobal J, Gallego J. Laboratory evaluation of the mechanical properties of asphalt mixtures with rubber incorporated by the wet, dry, and semi-wet process. *Construction and Building Materials*. 2019; 205: 164-174. doi:10.1016/j.conbuildmat.2019.01.159

[10] Zulkernain NH, Gani P, Chuck Chuan N, Uvarajan T. Utilisation of plastic waste as aggregate in construction materials: A review. *Construction and Building Materials*. 2021; 296: 123669. doi:10.1016/j.conbuildmat.2021.123669

[11] Awoyera PO, Adesina A. Plastic wastes to construction products: Status, limitations and future perspective. *Case Studies in Construction Materials*. 2020; 12: e00330. doi:10.1016/j.cscm.2020.e00330

[12] Sangeeta J, Khan TA, Rashid S, Sharma DK. Effect of waste polymer modifier on the properties of bituminous concrete mixes. *Construction and Building Materials*. 2011; 25(10): 3841-3848. doi:10.1016/j.conbuildmat.2011.04.003

[13] Vasudevan R, Ramalinga Chandra Sekar A, Sundarakannan B, Velkennedy R. A technique to dispose waste plastics in an ecofriendly way: Application in construction of flexible pavements. *Construction and Building Materials*. 2012; 28(1): 311-320. doi:10.1016/j.conbuildmat.2011.08.031

[14] Melbouci B, Sazdoun S, Bilek A. Study of the strengthening of recycled asphalt concrete by plastic aggregate. *International Journal of Pavement Research and Technology.* 2014; 7(4): 280-286. doi: 10.6135/ijprt.org.tw/2014.7(4).280

[15] Lastra-González P, Calzada-Pérez MA, Castro-Fresno D, Vega-Zamanillo Á, Indacoechea-Vega I. Comparative analysis of the performance of asphalt concretes modified by dry way with polymeric waste. *Construction and Building Materials*. 2016; 112: 1133-1140. doi:10.1016/j.conbuildmat.2016.02.156

[16] Angelone S, Cauhapé Casaux M, Borghi M, Martinez FO. Green pavements: Reuse of plastic waste in asphalt mixtures. *Materials and Structures* 2016; 49(5): 1655-1665. doi:10.1617/s11527-015-0602-x

[17] Schapery RA. Deformation and fracture characterization of inelastic composite materials using potentials. *Polymer Engineering and Science.* 1987; 27(1): 63-76.

[18] Underwood BS, Kim YR, Guddati MN. Improved calculation method of damage parameter in viscoelastic continuum damage model. *International Journal of Pavement Engineering*. 2010; 11(6): 459-476. doi:10.1080/10298430903398088

[19] Schapery RA. Correspondence principles and a generalized J integral for large deformation and fracture analysis of viscoelastic media. *International Journal of Fracture*. 1984; 25(3): 195-223. doi:10.1007/BF01140837

[20] Chebab GR, Kim YR, Schapery RA, Witczak MW, Bonaquist R. Time-temperature superposition principle for asphalt concrete with growing damage in tension state. *Journal of the Association of Asphalt Paving Technologists.* 2002; 71: 559-593.

[21] Underwood BS, Baek C, Kim YR. Simplified Viscoelastic Continuum Damage Model as platform for asphalt concrete fatigue analysis. *Transportation Research Record*. 2012; 2296(1): 36-45. doi:10.3141/2296-04

[22] Saleh NF, Keshavarzi B, Yousefi Rad F, Mocelin D, Elwardany M, Castorena C, Underwood BS, Kim YR. Effects of aging on asphalt mixture and pavement performance. *Construction and Building Materials*. 2020; 258: 120309. doi:10.1016/j.conbuildmat.2020.120309

[23] Wang YD, Keshavarzi B, Kim YR. Fatigue performance prediction of asphalt pavements with FlexPAVE[TM], the S-VECD Model, and D^R failure criterion. *Transportation Research Record*. 2018; 2672(40): 217-227. doi:10.1177/0361198118756873

[24] Wang YD, Ghanbari A, Underwood BS, Kim YR. Development of preliminary transfer functions for performance predictions in FlexPAVE[TM]. *Construction and Building Materials*. 2021; 266: 121182. doi:10.1016/j.conbuildmat.2020.121182

690 [25] D'Angelo S, Ferrotti G, Cardone F, Canestrari F. Asphalt binder modification with
691   plastomeric compounds containing recycled plastics and graphene. *Materials*. 2022; 15(2):
692   516. doi:10.3390/ma15020516

693 [26] Cardone F, Spadoni S, Ferrotti G, Canestrari F. Asphalt mixture modification with a
694   plastomeric compound containing recycled plastic: Laboratory and field investigation.
695   *Materials and Structures*. 2022; 55:109. doi: 10.1617/s11527-022-01954-4

696 [27] EN 12697-31: 2019. *Bituminous Mixtures - Test Methods - Part 31: Specimen Preparation*
697   *by Gyratory Compactor*.

698 [28] AASHTO R 83: 2017. *Standard Practice for Preparation of Cylindrical Performance Test*
699   *Specimens Using the Superpave Gyratory Compactor*.

700 [29] AASHTO PP 99: 2019. *Standard Practice for Preparation of Small Cylindrical*
701   *Performance Tests Specimens Using the Superpave Gyratory Compactor (SGC) or Field*
702   *Cores*.

703 [30] AASHTO T 378: 2017. *Standard Method of Test for Determining the Dynamic Modulus and*
704   *Flow Number for Asphalt Mixtures Using the Asphalt Mixture Performance Tester (AMPT)*.

705 [31] AASHTO TP 132: 2019. *Standard Method of Test for Determining the Dynamic Modulus*
706   *for Asphalt Mixtures Using Small Specimens in the Asphalt Mixture Performance Tester*
707   *(AMPT)*.

708 [32] AASHTO R 84: 2017. *Standard Practice for Developing Dynamic Modulus Master Curves*
709   *for Asphalt Mixtures Using the Asphalt Mixture Performance Tester (AMPT)*.

710 [33] Olard F, Di Benedetto H. General 2S2P1D model and relation between the linear
711   viscoelastic behaviours of bituminous binders and mixes. *Road Materials and Pavement*
712   *Design*. 2003; 4(2): 185-224. doi:10.1080/14680629.2003.9689946

713 [34] AASHTO TP 133: 2021. *Standard Method of Test for Determining the Damage*
714   *Characteristic Curve and Failure Criterion Using Small Specimens in the Asphalt Mixture*
715   *Performance Tester (AMPT) Cyclic Fatigue Test*.

716 [35] AASHTO TP 107: 2018. *Standard Method of Test for Determining the Damage*
717   *Characteristic Curve and Failure Criterion Using the Asphalt Mixture Performance Tester*
718   *(AMPT) Cyclic Fatigue Test*.

719 [36] Daniel JS, Kim YR. Development of a simplified fatigue test and analysis procedure using a
720   viscoelastic damage model. *Journal of the Association of Asphalt Paving Technologists*.
721   2002; 71: 619-650.

722 [37] Wang YD, Kim YR. Development of a pseudo strain energy-based fatigue failure criterion
723   for asphalt mixtures. *International Journal of Pavement Engineering*. 2019; 20(10): 1182-
724   1192. doi:10.1080/10298436.2017.1394100

725 [38] Wang YD, Underwood BS, Kim YR. Development of a fatigue index parameter, S_{app}, for
726   asphalt mixes using viscoelastic continuum damage theory. *International Journal of*

727   *Pavement Engineering*. 2022; 23(2): 438-452. doi:10.1080/10298436.2020.1751844

728   [39] Giuliani F. Definizione di una mappa nazionale di Performance Grade dei bitumi stradali.
729   *Quarry and Construction*. 2006; 527: 1-12 (in Italian).

730   [40] AASHTO T 331: 2021. *Standard Method of Test for Bulk Specific Gravity (G_{mb}) and*
731   *Density of Compacted Asphalt Mixtures Using Automatic Vacuum Sealing Method.*

732   [41] EN 12697-6: 2020. *Bituminous Mixtures - Test Methods - Part 6: Determination of Bulk*
733   *Density of Bituminous Specimens.*

734   [42] EN 12697-26: 2018. *Bituminous Mixtures - Test Methods - Part 26: Stiffness.*

735   [43] Castorena C, Kim YR, Pape S, Lee K. *Development of Small Specimen Geometry for*
736   *Asphalt Mixtures Performance Testing*. IDEA Program Final Report, NCHRP IDEA Project
737   N-181. 2017.

738   [44] EN 12697-24:2018. *Bituminous Mixtures - Test Methods - Part 24: Resistance to Fatigue.*

739   [45] Eslaminia M, Guddati MN. Fourier-finite element analysis of pavements under moving
740   vehicular loading. *International Journal of Pavement Engineering*. 2016; 17 (7): 602-614.
741   doi:10.1080/10298436.2015.1007237